

SCIENTIFIC REPORTS



OPEN

Liquid Marble as Bioreactor for Engineering Three-Dimensional Toroid Tissues

Raja K. Vadivelu^{1,2}, Harshad Kamble^{1,2}, Ahmed Munaz^{1,2} & Nam-Trung Nguyen ²

Liquid marble is a liquid droplet coated with hydrophobic powder that can be used as a bioreactor. This paper reports the three-dimensional self-assembly and culture of a cell toroid in a slow-releasing, non-adhesive and evaporation-reducing bioreactor platform based on a liquid marble. The bioreactor is constructed by embedding a hydrogel sphere containing growth factor into a liquid marble filled with a suspension of dissociated cells. The hydrogel maintains the water content and concurrently acts as a slow-release carrier. The concentration gradient of growth factor induces cell migration and assembly into toroidal aggregates. An optimum cell concentration resulted in the toroidal (doughnut-like) tissue after 12 hours. The harvested cell toroids showed rapid closure of the inner opening when treated with the growth factor. We also present a geometric growth model to describe the shape of the toroidal tissue over time. In analogy to the classical two-dimensional scratch assay, we propose that the cell toroids reported here open up new possibilities to screen drugs affecting cell migration in three dimensions.

Culturing cells in a three-dimensional (3D) format has been attracting attention from the research community due to the wide range of applications such as drug screening¹, high-throughput chemical analysis², disease models³ and, particularly cell transplantation for injury repair⁴. There is an urgent need for a technology that enables cells to grow in three dimensions in their native state without the restriction of supporting scaffolds, thus closely mimicking the natural *in-vivo* environment⁵. Currently, the most popular scaffold-free microfluidic concept for a 3D cell culture is growing spheroids in hanging drops⁶. Recently, high-throughput screening with cell spheroids has been achieved using the hanging drop concept⁷ and non-adhesive microwell arrays⁸. However, challenges remain for growing tissues with complex shapes⁹ such as toroids^{10–12}. Whilst each of previously reported scaffold-free methods is relatively easy to implement, they all have performance limiting factors. For example, hanging as well as sessile droplets are exposed to the atmosphere and evaporate quickly^{13,14}. Due to the evaporation, the culture medium disappears within hours and sets a time limit on the culturing process. This bottle neck will be solved, if the culture environment could be maintained for a much longer period.

Liquid marbles, liquid droplets coated with hydrophobic powder, have been recently used for culturing cells¹⁵. Evaporation of the culture medium still is a major problem of liquid marbles as a bioreactors. Sessile liquid marbles on a solid surface evaporate and collapse within hours¹⁴ and are not suitable for culturing cells over days and weeks. We have solved this problem previously by floating the marble on another liquid^{16–18}. The proximity to the liquid surface allows floating liquid marbles to maintain their integrity for days and weeks. This unique property makes floating liquid marbles extremely attractive for serving as a digital microfluidic bioreactor platform. Culturing cell spheroids has been successfully demonstrated in this system¹⁹. Moreover, a liquid marble can mimic the 3D microenvironment for cell growth. Adding drugs or soluble factor to the liquid marble can particularly influence self-assembly of cells to form larger aggregates.

The present paper reports another unique method to make a slow-evaporating liquid marble suitable for culturing 3D cell toroids. To date, the most common methods to engineer cell toroids are moulding with micro fabricated platform¹⁰, micro moulded hydrogels¹¹ and non-adhesive conical pegs¹². The mould allows the cells to aggregate into the toroidal shape. In this paper, we present a new method to allow cells to assemble by chemotaxis in a concentration gradient of growth factor. The key novelty of our method is the inclusion of a hydrogel sphere

¹School of Natural Sciences, Nathan Campus, Griffith University, 170 Kessels Road, Nathan, QLD 4111, Australia.

²Queensland Micro- and Nanotechnology Centre, Nathan Campus, Griffith University, 170 Kessels Road, Nathan, QLD 4111, Australia. Correspondence and requests for materials should be addressed to R.K.V. (email: raja.vadivelu@griffithuni.edu.au) or N.-T.N. (email: nam-trung.nguyen@griffith.edu.au)

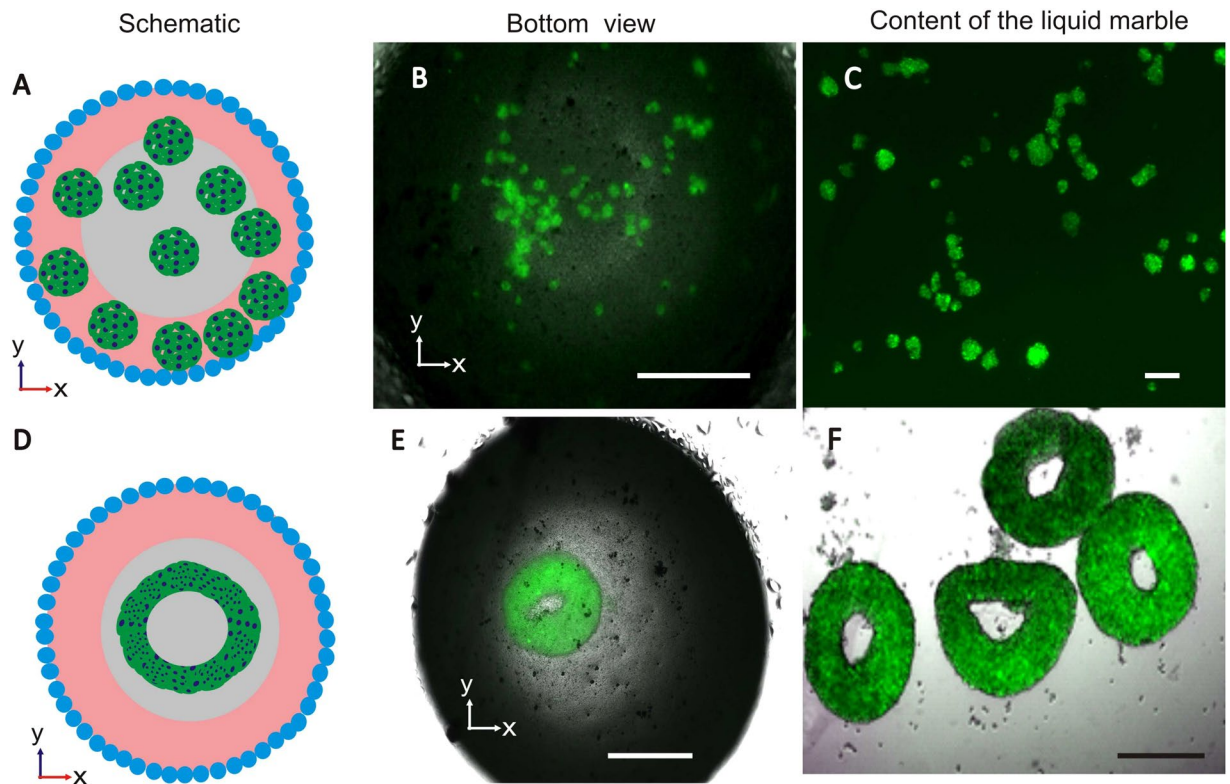


Figure 1. Physical properties of a liquid marble for the generation of spheroids and toroids (A) Schematic description of floating condition embedded with agarose hydrogel and the production of spheroids (bottom view). (B) Floating liquid marble producing multiple spheroids. (C) The morphology of spheroids harvested from several liquid marbles. (D) Schematic diagram showing toroid tissue generation inside a sessile LM (bottom view). (E) Toroid tissue formed inside a sessile marble. (F) The structure of toroids harvested from four sessile liquid marbles. Scale bar in (A) is 200 μm and (B,E and F) is 500 μm .

in the liquid marble. The hydrogel sphere serves as a storage of growth factor for slow release into the culture medium for sustainable growth of the 3D tissues. This platform offers additional controllability through careful manipulation of the marble motion, shape and composition of the hydrogel sphere, which in turn generates a concentration gradient of growth factor for chemotaxis. This platform allows for the growth of not only conventional cell spheroids but also more complex tissue geometries such as cell toroids. Cell toroids are tissues with a “doughnut-like” toroidal shape.

To date, drug screening for studying cell migration is predominantly carried out in a two-dimensional (2D) environment²⁰. Cell migration induced by drug or growth factor has been examined by simple 2D scratch migration assays or single-cell assays, which may not accurately replicate the 3D *in-vivo* environment^{21,22}. In contrast, a 3D tissue model has recently gained increasing interest in studying cell migration^{23,24}, regeneration²⁵, and repair²⁶. A 3D model matches the mammalian tissue niche morphologically and physiologically. At the cellular level, a 3D environment supports complex cell-matrix interaction and maximizes the cell-cell interaction²⁷ that closely emulate what cells in native tissue environment experience²⁸. Additionally, the reorganization of actin cytoskeletal and cell-matrix adhesion is prerequisite for cells to adhere to the matrix and to exert contractile force to move forward. The cytoskeletal mediated tension in a 3D model leads to different migration speeds and patterns than that of a 2D model²⁸. Moreover, scaffold-free 3D cultures are comprised of cells in spatial arrangement and leads to the synthesis of permissive ECM components²⁹. Thus, 3D models enable the detailed analysis of the interaction between an active chemical substance and a biological system. This type of analysis is often required for *in vivo* toxicity analysis and drug screening. Recently, 3D cell-based anti-invasive and migration assays have gained tremendous interest in drug discovery because they can solve the known problem of discrepancies between the behaviour of cells on a flat substrate and *in vivo*³⁰. However, quantitative analysis and microscopic imaging of the morphodynamics during cell migration in a 3D tissue is technologically difficult. To address this challenge, we propose a toroid shaped tissue that is easily adaptable for 3D cell migration analysis using direct imaging of the inner opening closure.

At the molecular level, ligand and membrane receptors of cells in a 2D model are exposed evenly per unit area. In contrast, a 3D tissue has tightly packed clusters and more complex configurations³¹. Moreover, drug or soluble factors induce signal transduction and influence the cellular behaviour in three dimensions differently, because cellular topographic sensing is affected by spatial organization of the tissue³². Thus, in term of drug exposure, 3D models are obviously advantageous in predicting the response of cells to drug. To date, 3D cell migration assays are limited to embedding cells into a matrix^{33–35}, fabrication of cells with biomaterials scaffolds^{36–38} or tissue ring

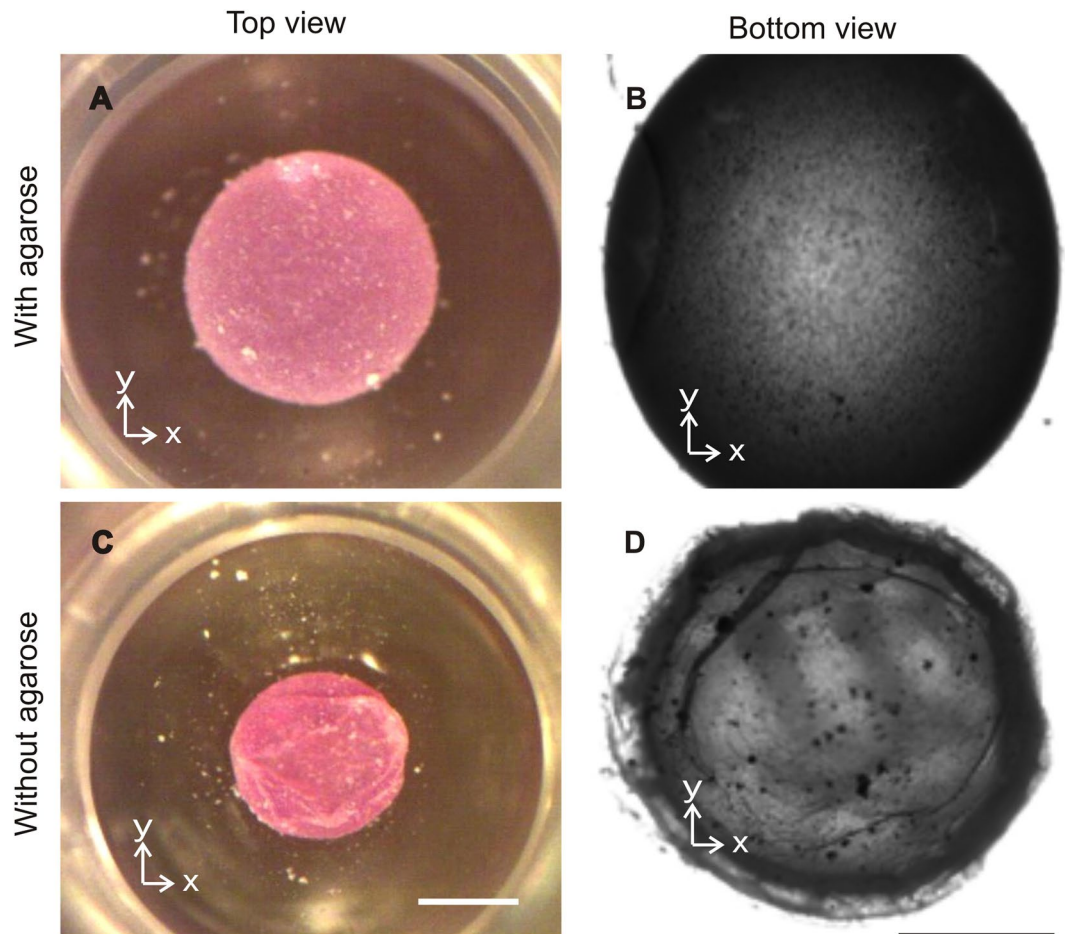


Figure 2. Effect of evaporation on a sessile liquid marble: (A) Top view of a sessile liquid marble with embedded agarose hydrogel. (B) Bright field image of a liquid marble containing agarose gel. The surface of the liquid marble did not show wrinkles. (C) Top view of a shrunken sessile liquid marble without agarose hydrogel. (D) Wrinkles on the surface indicating excessive evaporation. The total volume of the liquid in the marble is $10\ \mu\text{L}$. Scale bars are $500\ \mu\text{m}$.

closure using magnetic levitation³⁹. The present paper reports a 3D model with toroidal geometry that is formed through self-assembly of cells.

Furthermore, we demonstrate here the ability of olfactory ensheathing cells (OECs) to migrate from a toroidal multicellular tissue by evaluating the rate of closure. OECs have been considered as the potential candidates for transplantation therapy following a spinal cord injury (SCI)^{40,41}. The potential challenge of OEC-based therapy is enhancing the survival rate and the migration of OECs after the transplantation⁴². The migration of OECs is vital for the regeneration of neurons. As neurotrophic factors can promote the migration of OECs^{43–45}, we employed glial derived neurotrophic factor (GDNF) in the experiments to promote cell migration and to evaluate the closure rate of the cell toroid.

Concept of slow evaporation

We address the evaporation problem by including a hydrogel sphere inside the sessile liquid marble. Preliminary experiments indicated that a floating liquid marble with a hydrogel sphere rapidly form spheroids, similar to the case of a floating liquid marble without embedded hydrogel¹⁹. A floating liquid marble behaves like a Leidenfrost drop⁴⁶ and creates an internal flow that disperses the cells and let them interact freely to form multiple spheroids, Fig. 1A–C. In contrast, a sessile liquid marble on a solid surface generates toroid tissue. The formation of the toroid tissue is based on both chemotaxis and gravity driven self-assembly of cells around the bottom of the hydrogel sphere, Fig. 1D–F.

Embedding a hydrogel sphere inside the liquid marble can slow down evaporation. A liquid marble containing a sphere made of agarose as the hydrogel maintains after 24 hours its spherical shape without significant wrinkles on the hydrophobic coating, Fig. 2A,B. In contrast, a sessile liquid marble lost its liquid content, shrunk and formed wrinkles after 24 hours, Fig. 2C,D. A sessile liquid marble suffers from excessive evaporation, which limits the life time of the cell culture. This phenomenon indicates that the embedded hydrogel sphere limited evaporation.

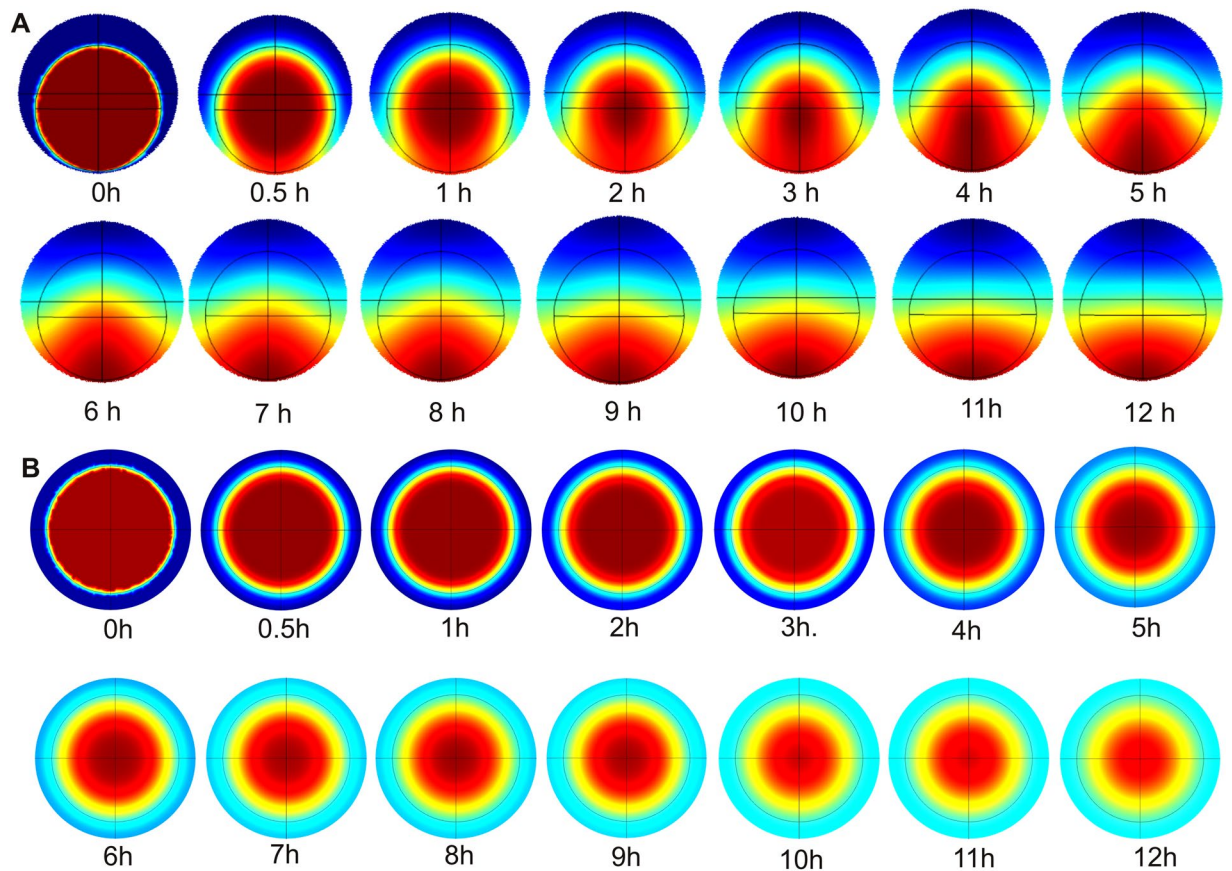


Figure 3. Simulated concentration distributions of growth factor over time inside the liquid marble through slow release from the embedded hydrogel sphere. (A) Volumes of the hydrogel sphere and the liquid marble are $3\ \mu\text{L}$ and $5\ \mu\text{L}$, respectively. The diffusion coefficient of growth factor in both hydrogel and medium is assumed to be the same and has a value of $D = 10^{-7}\ \text{cm}^2/\text{s}$. In the initial state (0 min), red indicates the hydrogel sphere; blue indicates the medium seeded with cells. (B) The same simulation was carried out for a hydrogel sphere positioned in the centre of the liquid marble. The radial concentration distribution is uniform.

Concept of slow release

We first numerically estimated the effect of diffusion in the liquid marble/hydrogel platform. The model predicts the concentration distribution of the growth factor inside the marble in three dimensions. The formation process of the toroid tissue is constrained in the space between the hydrogel sphere and the shell of the liquid marble. In the present work, we used epidermal growth factor (EGF), which is well characterized and known for promoting cell migration. Numerous previous studies have reported the use of EGF for *in vitro* release from encapsulated hydrogel^{47–49}.

Taking the Fick's diffusion law into account, the diffusion time of the growth factor in a spherical liquid marble, or the time to have the growth factor equally distributed inside the marble, can be estimated as⁵⁰:

$$t_d = r_{\text{LM}}^2/6D \quad (1)$$

In our experiments, a $10\text{-}\mu\text{L}$ liquid marble has a radius of $r_{\text{LM}} = 1.34\ \text{mm}$. Assuming a diffusion coefficient of the growth factor of $D = 10^{-7}\ \text{cm}^2/\text{s}$ ⁵¹, the release time of the growth factor is estimated to be $t_d \approx 8.27\ \text{h}$. Thus, the cells should have enough time in the first few hours to aggregate around the high concentration next to the hydrogel sphere.

Next, we conducted a 3D numerical simulation (COMSOL Multiphysics, COMSOL, Inc., USA) of the diffusion process of the growth factor to predict the location of the cell aggregates. Figure 3A shows the model and the corresponding concentration distribution over time. Red and blue colours indicate high and low concentration, respectively. The initial condition is the uniform concentration of growth factor inside the hydrogel sphere. The embedded hydrogel sphere is placed on the centre axis of a sessile liquid marble. The remaining space in the liquid marble is restricted by the hydrogel sphere and the non-adhesive shell (blue area in Fig. 3A, 0 min). This configuration represents the miniaturized 3D version of the conventional 2D “under agarose assay”. Figure 3A shows that the agarose sphere also serves as a reservoir to sustain the slow release of growth factor and water. The well-controlled high concentration of chemoattractant allows cells to migrate into a ring-like aggregate under the hydrogel sphere. According to the simulation, the higher concentration of growth factor at the bottom of the liquid marble can be maintained even after 12 hours of cell culture, when the tissue is ready to be harvested. As reference, the concentration field around a hydrogel sphere placed at the centre of the marble shows an expected

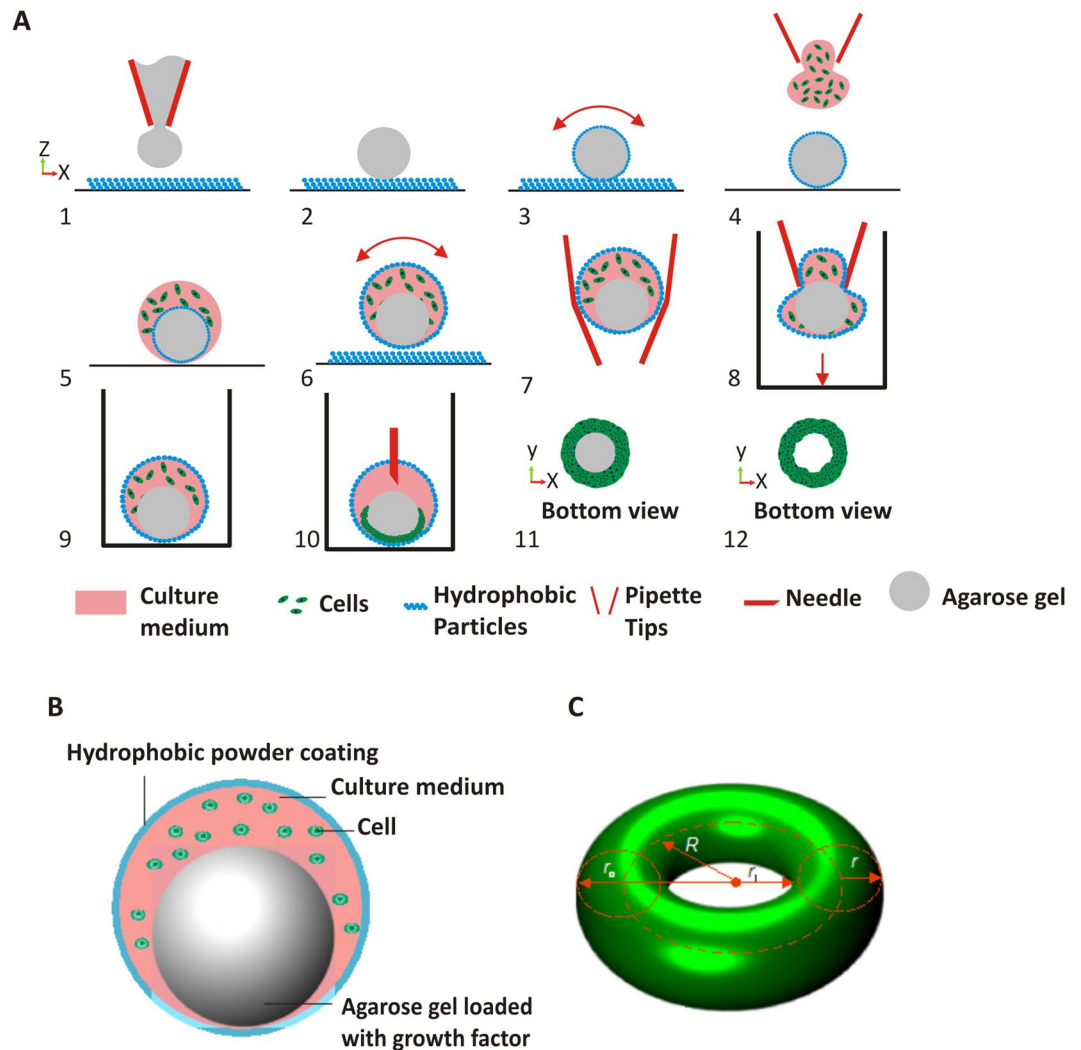


Figure 4. The bioreactor model, geometry of a toroid tissue and procedure for generating bioreactor platform for toroid tissue growth: (A) (1,2) Dispensing a hydrogel droplet on the powder bed. (3) Rolling the hydrogel droplet to coat it with hydrophobic powder. (4) Impacting an aqueous medium droplet containing cells on the hydrogel. (5) Encapsulating the hydrogel liquid marble with the medium and seeded cells. The hydrophobic powder of the hydrogel marble automatically migrates to the liquid/air interface of the larger droplet. (6) The composite liquid marble is rolled on the hydrophobic powder to ensure sufficient coating for maintaining its robustness. (7,8) The marble is picked up and transferred using a pipette tip and placed on 96 well plate. (9) A slow-evaporating liquid marble with cells and hydrogel for slow release of growth factor, ready for incubation. (10) After incubation, the cells settled and migrated at the bottom of the liquid marble to form toroidal tissue construct. (11) Marbles can be broken with needles to release the toroid tissue. (12) The toroid tissue and the agarose gel at the bottom of the well are separated for further analysis. (B) A liquid marble with embedded hydrogel sphere. (C) The basic geometry of a toroid (major radius R , minor radius r , inner radius $r_i = R - r$, volume $V = 2\pi^2 R r^2$, surface area $A = 4\pi^2 R r$, aspect ratio $\alpha = R/r$).

uniform radial distribution over time, Fig. 3B. Thus, the distribution in Fig. 3A is unique for the sessile liquid marble used for growing the cell toroid described in the next section.

Growing of toroidal tissue

The key innovation of the platform reported here is the embedded hydrogel sphere. To start with, a 0.5% low melting (37°C) agarose containing growth factors at $5\text{-}\mu\text{L}$ volume was coated with polytetrafluoroethylene (PTFE) powder with an average particle size of $1\text{ }\mu\text{m}$ (Sigma-Aldrich, product number 430935) by dispensing the gel onto the powder bed, Fig. 4A1,2. The agarose droplet was rolled in a circular motion to ensure that the PTFE powder covered the surface evenly, Fig. 4A3. After 3 to 5 minutes, the agarose droplet solidifies to form a sphere. This critical step ensures that the agarose spheres are consistent in size. Subsequently, a second droplet containing a predetermined number of OECs in the volume of $10\text{ }\mu\text{L}$ was injected to collide with the top of the agarose to form a single droplet containing cells and agarose, Fig. 4A4. By adjusting the pipetted volumes, liquid marbles

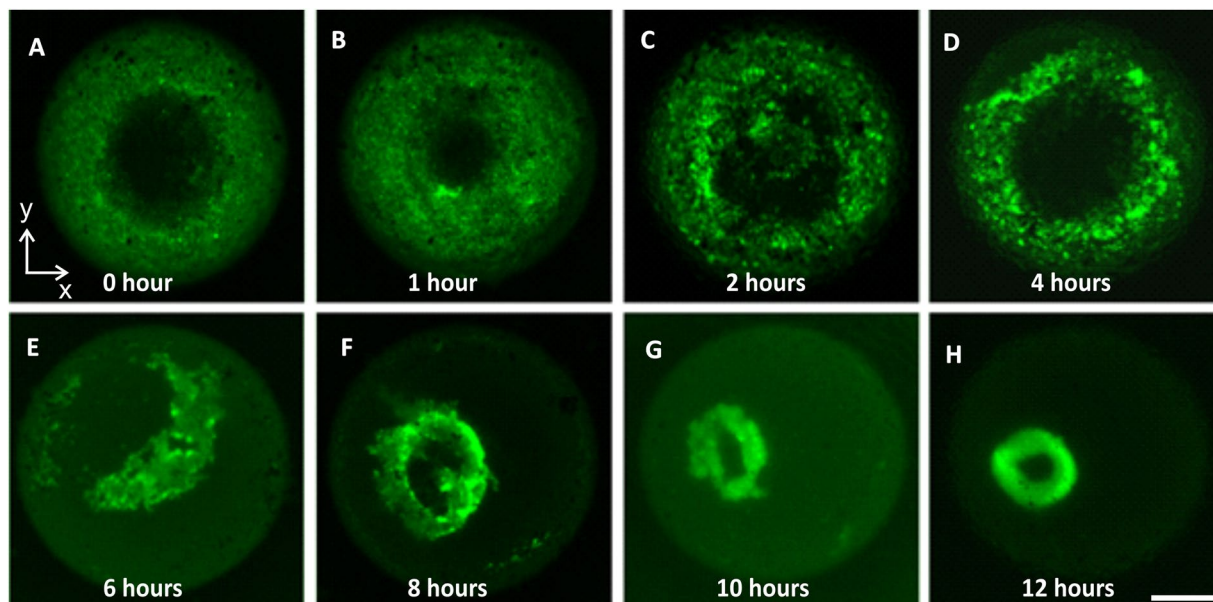


Figure 5. The formation of toroidal tissue inside liquid marble over time. Scale bar is 500 μm .

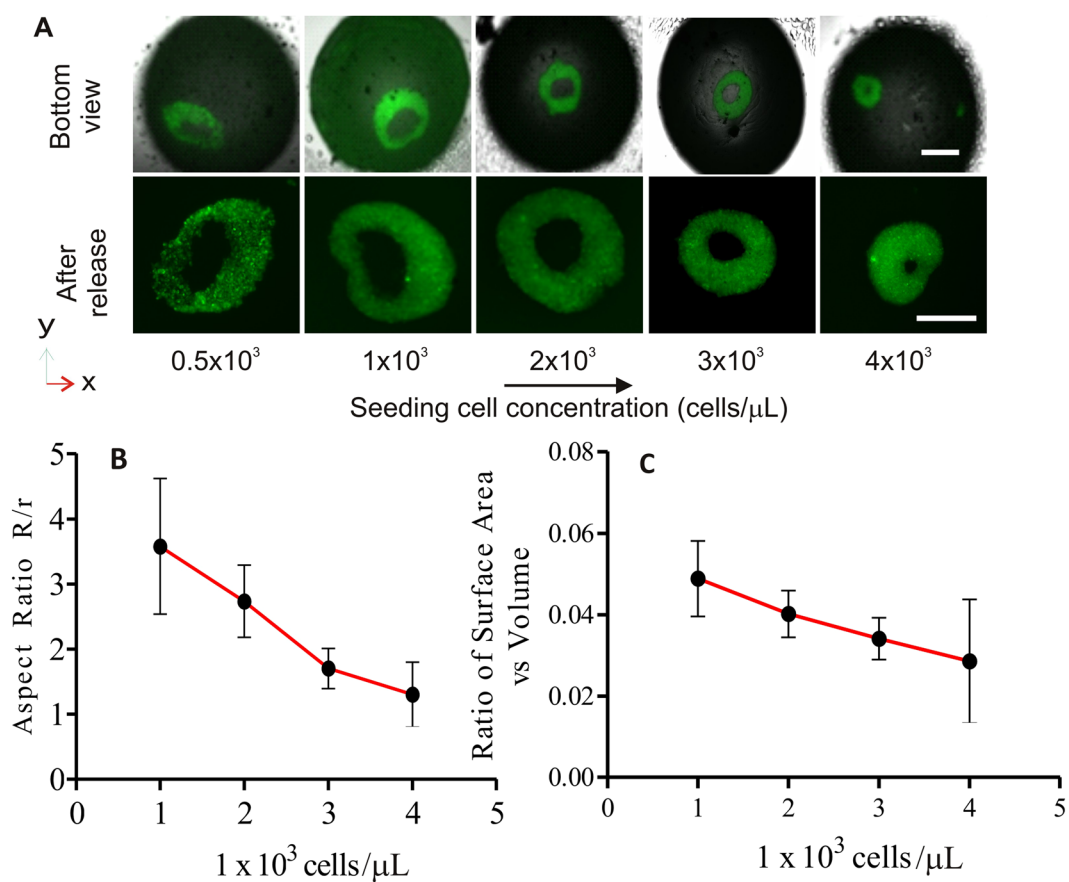


Figure 6. The role of seeding cell concentration: (A) Toroids with different seeding cell concentrations. (B) Aspect ratio as function of seeding cell concentration. (C) Surface area to volume ratio as function of seeding cell concentration. All experiments were repeated three times with $n = 5$ toroids each. Bars represent the mean; error bars represent the standard error of the mean. The scale bar inside the liquid marble is 500 μm and the harvested toroid is 200 μm .

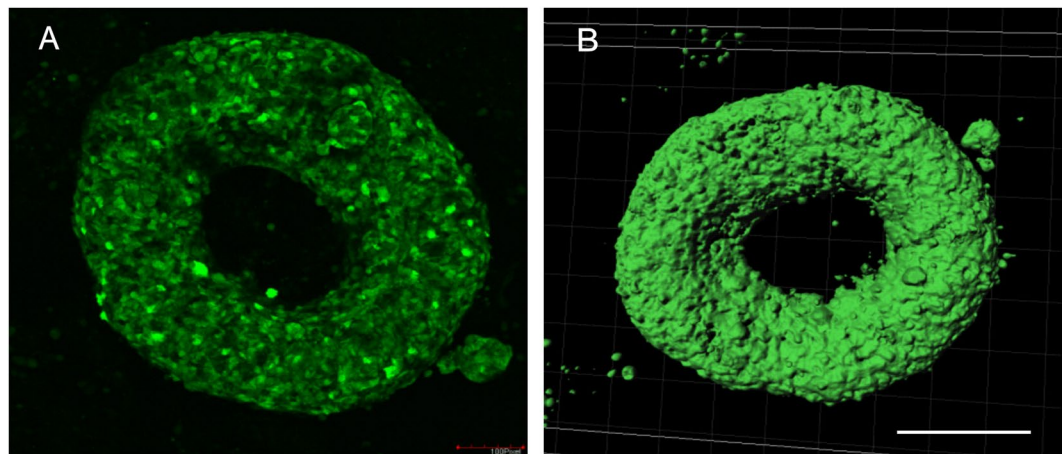


Figure 7. Morphology of a cell toroid: (A) A single confocal slice of the toroid. (B) The assembled 3D image indicates a toroidal shape. Scale bar is 200 μm .

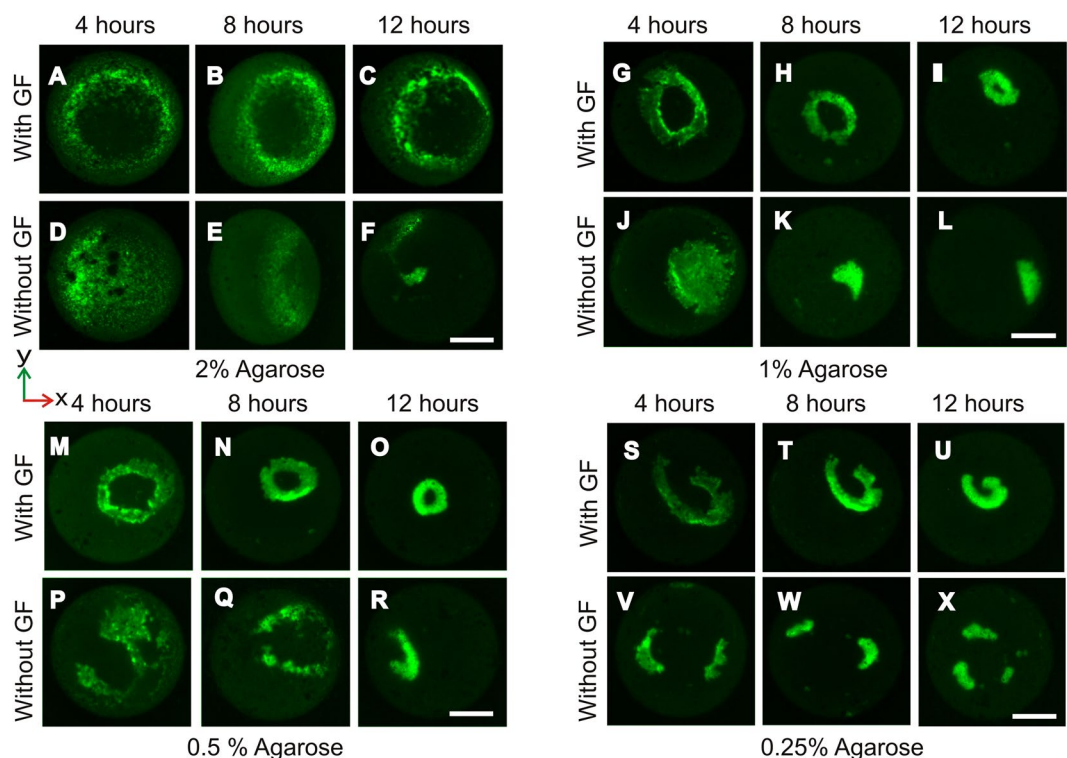


Figure 8. The role of agarose and growth factor in toroid formation. The release of growth factor and cell assembly to form of cell toroids from 4 to 12 hours (A–C). Toroid formation was disrupted at 2% agarose with growth factor. Irregular toroidal tissues are formed at 1% agarose (G–I) and at 0.25% agarose (S–U). The ideal toroid was formed with 0.5% agarose containing growth factor (M–O). Cells did not assemble into toroid in all conditions without growth factor. The scale bar is 500 μm .

with a volume ranging from 2 to 50 μL can be formed. For consistency, we kept the volume in this study constant at 10 μL . The hydrophobic particles on the agarose hydrogel is stable at the liquid/air interface. Once the contact between the liquid and the hydrogel is made (Fig. 4A5), the particles migrate toward the outer liquid/air interface. As a result, the hydrogel marble and the cell marble merge to create a composite liquid marble. Next, we gently rotated the composite droplet to create a robust liquid marble containing both cells and the agarose sphere, Fig. 4A6. Since the liquid marble is elastic, a cut 1000- μL pipette was used to handle the marble. The pipette was able to suck and hold the marble, Fig. 4A7. The marble was then dispensed into a U-bottom 96-well plate Fig. 4A8. The liquid marble was kept in the sessile condition for 12 hours and incubated at 37 $^{\circ}\text{C}$, Fig. 4A9. The small particle size of the 1- μm PTFE powder creates a thin, porous coating, which allows for real-time observation of the assembly process of the cells. This protocol is suitable for the use of time-lapse microscopy to access the behaviour

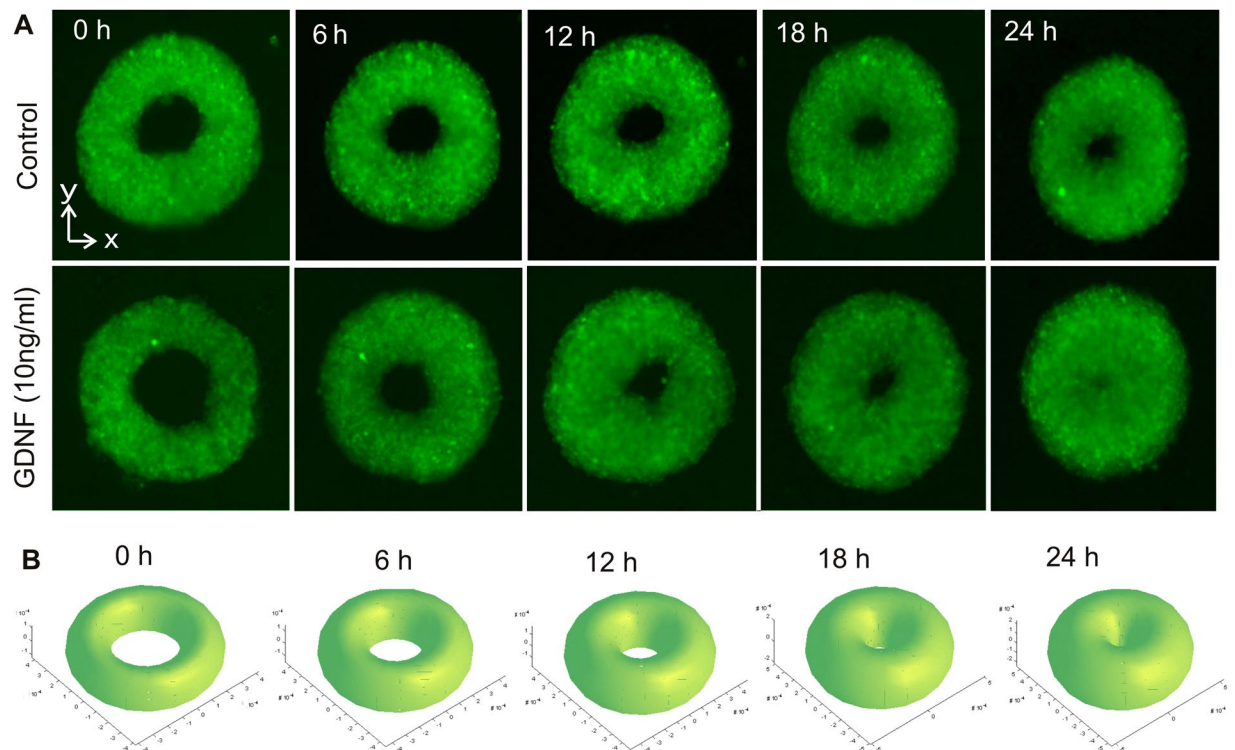


Figure 9. The effect of glial cell-derived neurotrophic factor on the closure process of a cell toroid: (A) Toroidal shapes over time. (B) The geometric model of the closure process with a constant growth rate ($R = 300 \mu\text{m}$, $r_0 = 120 \mu\text{m}$, $k = 5 \mu\text{m/hr}$). Scale bar is $200 \mu\text{m}$.

of toroidal tissue with different fluorescent labels. Finally, breaking the liquid marble (Fig. 4A10,11) releases the cell toroids which are subsequently seeded onto 96-well plates for further analysis Fig. 4A12. Figure 4B illustrates the schematic of the hydrogel/liquid marble bioreactor. Figure 4C shows the basic geometric parameters of the cell toroid, that were later used for its characterisation.

Formation process of the cell toroid

Next, we investigated the mechanism that governs the self-assembly of cells to form the cell toroid, particularly to understand the relationship between tissue shape and tissue deformation. We observed the cell-cell interaction by imaging the liquid marble at different instances. After about 30 minutes, the cells aggregate at the bottom of the liquid marble due to gravity and chemotaxis, Fig. 5A,B. The cells assembled at the lower surface of the liquid marble. Subsequently, between 2 and 4 hours, the cells attract each other and aggregate into a ring shape around the agarose sphere, Fig. 5C,D. Within 6 to 8 hours, the cell aggregates underwent two steps. In the first step, cell aggregates migrate underneath the agarose towards the bottom of the liquid marble, Fig. 5E. During this time, the inner shape of the toroid was still not completed, Fig. 5F. The second step is the self-assembly of cells into small unit blocks, which subsequently fuse into a thin toroid, Fig. 5G. Between 10 and 12 hours the tissue contracted significantly and formed a perfect toroid, Fig. 5H. Cell assembly and compaction under the surface tension contributes to the formation of the toroidal shape, which has a perfect circular opening.

The role of seeding cell concentration

We next quantified the effect of seeding concentration on the formation of a cell toroid. The ability of cells to self-assemble into a toroid depends on the number of viable cells and the concentration of the growth factor. We performed experiments with a fixed volume of $10 \mu\text{L}$ medium and $5 \mu\text{L}$ of 0.5% agarose solution, to determine the optimal cell concentration for the geometry of the final toroid. Cells were seeded with concentrations ranging from 0.5×10^3 to 4×10^3 cells/ μL . The tissue was allowed to assemble for 12 hours, Fig. 6A. The liquid marble was subsequently broken to release the cell toroids for measuring the geometric parameters such as the inner radius r_i , the minor radius r , and the major radius R , Fig. 4C.

A concentration of 1×10^3 cells/ μL resulted in a thin toroid and a large surface area to volume ratio. Eventually, cell concentration of less than 1×10^3 cells/ μL did not result in a uniform distribution. Therefore, the cells aggregated into irregular shapes or thin toroids that are prone to rupture. Figure 6B shows the aspect ratio R/r as a function of the cell concentrations, indicating a thicker toroid with a larger minor radius r and an almost constant major radius R . As the major radius R is determined by the constraining geometry of the liquid marble and the agarose sphere, this parameter does not vary with the concentration of the cells. However, the minor radius r depends on how fast the cells assemble and grow, thus depending on the cell concentration. A higher

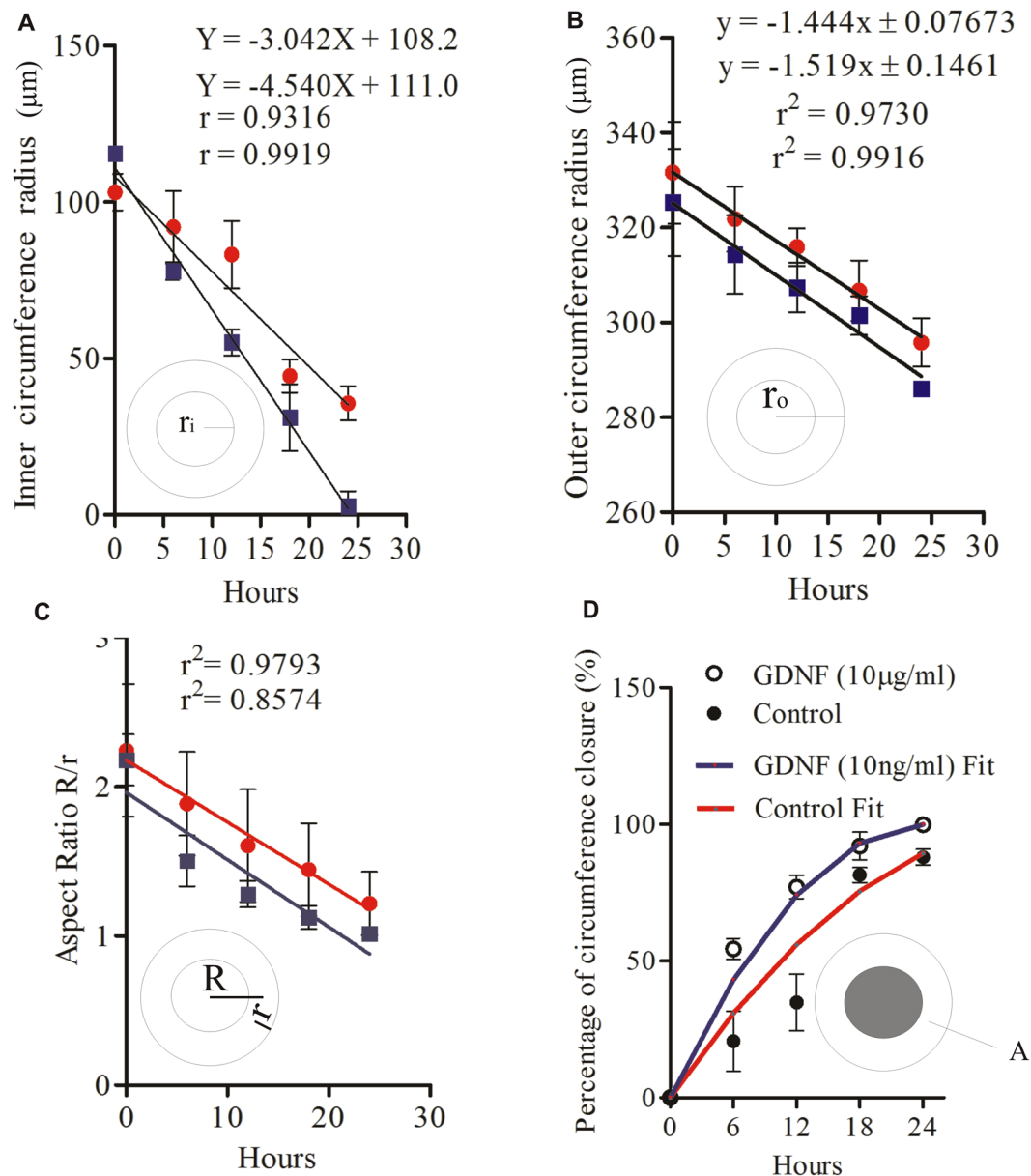


Figure 10. The effect of GDNF on the geometric parameters of the toroid. (A) Inner radius over time. (B) Outer radius over time. (C) Aspect ratio over time. (D) Percentage of cavity closure areas over time. Lines are fitting functions based on the respective linear models of (4), (7) and (8). All experiments were repeated three times with $n = 3$ toroids each. Bars represent the mean; error bars represent the standard error of the mean.

cell concentration results in a higher growth rate and a thicker toroid over the same culturing period. This result indicates that a significant number of cells are crucial for adjacent cells to self-assemble into a toroid.

Figure 6C depicts the relationship between the ratio of surface area versus volume and the cell concentration. The surface area and volume are calculated according to the geometry of a torus depicted in Fig. 4C. The outer radius of the toroid did not significantly vary with increasing cell concentration, suggesting that the space between the hydrogel sphere and the shell determines the outer shape of the toroid. The inner radius r_i decreases with increasing cell concentration leading to a lower surface area to volume ratio. At a concentration of 5×10^3 cells/ μL , the cells migrate, compact and take up a spherical shape. The seeding concentration of 2×10^3 cells/ μL produces cell toroid with a surface area to volume ratio of approximately 0.04.

The criteria for an ideal toroid are as follow. (i) The toroid should have the largest surface area per unit volume for making efficient diffusion of nutrient and effectively dispel waste from the inner core. (ii) The opening should be symmetric because its diameter is critical for the use of the toroid as a 3D wound healing model. At a lower cell density ($0.5\text{--}1 \times 10^3$ cells/ μL), we obtained toroid tissue with a higher surface area per unit volume but the tissues were irregular in shape. Further increasing the cell density to 3 and 4×10^3 cells/ μL produces thicker toroids with a

smaller inner radius. A thicker toroid may affect the tissue viability. Thus, in our subsequent experiments, the optimal number of cells necessary to display a symmetrical, stable and functional toroid is 2×10^3 cells / μL , Fig. 7A,B.

The role of agarose concentration

We created agarose spheres with a concentration between 0.25 and 2% with and without growth factor, to elucidate the contribution of agarose in the formation of the toroidal tissue. Particularly, we aimed to determine whether the toroid formation is caused by cell sedimentation at the bottom of the liquid marble. The formation of the toroid was observed with these agarose spheres at 4, 8 and 12 hours, Fig. 8. Surprisingly, cells did not assemble to form toroid in the absence of growth factor under all conditions. Furthermore, a high concentration of agarose of 2%, eventually failed to create a cell toroid even with growth factor, Fig. 8A–C. The cells did not migrate under the agarose and exhibit a poor rate of cell assembly, especially at 12 hours. Cell aggregates were not uniformly distributed in a circular pattern at 4 hours in the absence of growth factor.

Interestingly, cells assembled under the agarose sphere to form the toroidal shape at agarose concentrations of 0.5 and 1%. However, we did not observe any obvious differences between these concentrations. An ideal toroidal shape was observed with the agarose concentration of 0.5%, Fig. 8M–O. A lower agarose concentration of 0.25% results in an irregular toroidal shape with a larger inner radius, Fig. 8S–U. This observation further supports the role of agarose in stimulating cell aggregation and assembly by the slow release of growth factor through the diffusion process. The release process depends on the concentration of the agarose and the corresponding porosity. The pore size of an agarose gel increases with decreasing concentration. Thus, 0.5% agarose is optimal for diffusion. Higher or lower agarose concentrations may release growth factor too slow or too fast for the required cell assembly.

The sedimentation of cells inside the LM and the subsequent formation of cell toroids are facilitated by the following mechanisms: (i) gravity enforced assembly of cells, (ii) cell-cell cohesion, (iii) chemotaxis due to growth factor release from the agarose. After an initial incubation time, the seeded cells settled at the bottom of the liquid marble. Subsequently, the cells aggregate and assemble into a ring shape around the lower region of the agarose sphere. In the absence of growth factor, cells aggregate into irregular clusters. As shown in the numerical simulation, the growth factor concentration is higher at the lower hemisphere of the liquid marble. The high concentration of the growth factor direct the cell migration and enhance cell-to-cell adhesion around the bottom of the agarose gel. As a result, cell-cell interactions contributes to cell contraction and self-assemble into a toroid. We also found that the opening of the toroid did not match that of the diameter of the agarose sphere. In fact, the diameter of the opening decreases with increasing cell concentration. Thus, we hypothesise that the contribution of the growth factor to the formation of the toroid dominate over the gravity effect and the surface properties of the agarose.

Closure of the 3D toroidal tissue

We use a geometric growth model to predict the tissue closure based on a constant linear growth rate. The measure of lumen closure is the instantaneous value of appreciable cell migration, which models the mechanism of wound closure in three dimensions. Figure 9 shows the closing process of a cell toroid after harvesting them from the liquid marble/agarose bioreactor. Figure 9A indicates that glial cell-derived neurotrophic factor (GDNF) increases the percentage of inner circumference closure at a time instance between 6 to 24 hours as compared to the control. The data indicate that the closure of toroid lumen progressively increase from 0 to 12 hours, suggesting that in early stage cells actively migrate instead of proliferation. Subsequently, the closure rate decreased, and complete lumen closure occurred between 18 to 24. At this stage, the cell population may involve both cell migration and proliferation. Previous investigation indicated that mitotically active cells depends on cell doubling time, which are prominent and persist 24 h after wounding⁵². Moreover, the outer diameter of the toroid in our study decreases over time and did not show evidence of outward spreading. These observations allow us to hypothesise that cell migration is actively involved, evidently through the persistent closing of the lumen. In addition, the wound closure rate is chemotactically driven by GDNF, which is known to induce OECs migration⁴⁴, but not proliferation⁵³. In this regards, cell migration can be the dominant mechanism, and cell proliferation is assumed to be a secondary event during the lumen closure process.

The geometric model for interpreting the experimental data of Fig. 9A assumes a linear growth rate in the radial direction of the minor radius $r(t)$:

$$r(t) = r_0 + kt \quad (2)$$

where r_0 is the initial minor radius of the toroidal tissue and t is the time. The growth rate k depends on the culture medium, e.g. the concentration of the growth factor and the cell concentration. The existence of growth factor contributes to a higher growth rate. The time dependent shape of the surface of the toroid can then be described based on the geometry as follows:

$$x(t) = [R + r(t)\cos\theta]\cos\varphi \quad (3)$$

$$y(t) = [R + r(t)\cos\theta]\sin\varphi \quad (4)$$

$$z(t) = r(t)\sin\theta \quad (5)$$

where θ and φ are the rotating angle around the minor and major axis of the toroid, respectively. Figure 9B shows the closure process of a representative toroidal tissue with a major radius $R = 300 \mu\text{m}$, initial minor radius $r_0 = 120 \mu\text{m}$ and a grow rate of $k = 5 \mu\text{m/hr}$. The results indicate that the geometric model with a linear growth rate

describes well the observed process depicted in Fig. 9A. To confirm the linear model, we evaluated the geometric parameters of the toroidal tissue for both control and GDNF over time.

Figure 10A shows the inner radius $r_i = R - r$ or the cavity radius as a function of time. A clear linear behaviour could be observed in both control and GDNF. Figure 10B shows the outer radius of the toroid as a function of time, indicating the overall shrinking of the cell toroid. In contrast to the linear growth model, the outer radius of the toroid decreases linearly over time, indicating continuous compaction of the tissue. Linear behaviour is reflected well in the aspect ratio of the toroidal tissue, Fig. 10C. Assuming that a cell toroid with an inner radius of $r_{i,0} = (R - r)_0$ grows in a radial direction at a constant rate k (Equation 3), the function of the inner radius over time t is:

$$r_i(t) = r_{i,0} - kt \quad (6)$$

Thus the cavity closure as a function of time can be estimated as:

$$\alpha = \frac{A_0 - A(t)}{A_0} \times 100\% = [1 - (1 - kt/r_{i,0})^2] \times 100\% \quad (7)$$

where A_0 and $A(t)$ are the initial cavity area and the time dependent cavity area, respectively. The inner radius grows radially inward at a constant rate k (Equation 3). The closure rate k can be determined from the measurement of the inner radius and a linear fit over time. The closure rates of the control experiments and experiments with GDNF are 3.04 $\mu\text{m/hr}$ and 4.54 $\mu\text{m/hr}$, respectively. As mentioned above, the outer diameter of the toroid decreases over time, but at a lower rate than the closure rate. The outer radius decreases at a rate of 1.44 $\mu\text{m/hr}$ and 1.52 $\mu\text{m/hr}$ for control and GDNF, respectively, Fig. 10A,B. The reason for the shrinking behaviour of the outer diameter could be the compaction of the tissue to minimize its overall surface area as a result of the closure. Figure 10D shows the evaluated cavity closure (7) of both cases over time. Clearly, GDNF has contributed to a faster closure of the cell toroid.

Discussion

First, we demonstrated the use of a liquid marble with embedded hydrogel as an ideal bioreactor platform to engineer cell toroid and its application as a 3D wound closure assay. The embedded hydrogel maintains the water content critical for culturing cells. Most microfluidic cell culture platforms use a small volume of liquid, and therefore evaporation is a major problem even in a humidified environment. Moreover, evaporation in a small volume affects the osmolality of the extracellular environment that alters the biochemical balance and impedes cell growth⁵⁴. The hydrophobic and porous shell of a liquid marble is permeable, allowing for the gas exchange that is vital for cell culture. At the same time, this porous shell makes it prone to evaporation. Our system uses a hydrogel sphere as the water storage⁵⁵ to reduce evaporation.

Second, the hydrogel sphere facilitates growth factor release and attracts cells to settle on the bottom of the liquid marble in a ring. In an aqueous environment, hydrogel swells by absorbing water and simultaneously release loaded solutes. Their porosity permits loading of the drug or growth factor. The released molecules diffuse to the surroundings, allowing slow drug release^{56,57}. Our optimization experiments indicated that a liquid marble seeded with 2×10^3 cells and 0.5% agarose containing growth factor resulted in an ideal toroid shape in just 12 hours. Hydrogels with larger pores cause premature dissolution or rapid drug release in a shorter time span. Our experimental data confirm this hypothesis. At an agarose concentration of 2.5%, we did not observe toroid tissue formation. Furthermore, at this concentration, the agarose may deform and do not maintain a spherical shape due to the lower interfacial tension relative to its weight.

Third, the bioreactor platform is sufficiently sensitive for the assessment of chemotaxis induced self-assembly of cells. Chemotactic stimuli display signal transduction events that activate directed cell migration as collective units^{58,59}. An organized migration toward external cues is critical for cells to aggregate into a uniform ring-like pattern, only 4-6 hours after seeding. In a liquid marble containing agarose without growth factor, cells are not able to migrate effectively. Experimental data show a decrease in cellular cohesion and non-homotypic aggregation. This observation evidently validates the hypothesis that cells undergo cluster attraction and migrate along the gradient of the growth factor. We formulated and carried out a numerical simulation of the concentration distribution of growth factor over time and found an agreement with chemotaxis-driven cell aggregation in our experiments. In addition to chemotaxis, cytoskeletal mediated tension/contraction contributes directed self-assembly to form a complex toroidal microtissues⁶⁰.

Fourth, our bioreactor platform allows for the regulation of the size of a cell toroid using the seeding concentration. Appropriate seeding concentration is crucial for obtaining the ideal toroid geometry due to the higher assembly or growth rate. Non-axisymmetric toroidal shapes are possible at low cell concentration. In contrast, a lower aspect ratio of approximately 1.0 was observed at a higher seeding concentration. The observation confirms that seeding concentration influences the migration and aggregation dynamics. Geometric parameters of cell toroid such as volume, surface area, minor and major radii are critical for tissue viability and functionality. For instance, a toroid with a large surface area to volume ratio is desirable, as sufficient nutrient diffusion and supporting metabolites can reach the interior milieu of intact cells. Moreover, enhanced solubility and stimuli of growth factor are mediated by abundant cell-surface receptors, which promote cell signalling and tissue growth. Interestingly, we identified a toroid with surface-area-to-volume ratios as high as 0.04 at a cell concentration of 2×10^3 cells/ μL could conserve appropriate function for wound healing or 3D cell migration assay.

Finally, we demonstrated that the cultured cell toroid serves well as a 3D wound closure assay. Rapid closure of the toroid inner circumference was achieved if the tissue was treated with 10 ng/ml growth factor. Experimental

data agreed well with the model of a constant closure rate. Toroidal tissues treated with growth factor clearly showed a higher closure rate than that without growth factor.

Outlook. The bioreactor platform reported here is useful for studying drug stimuli on cell sorting, cell-cell interaction and self-assembly to engineer the 3D unit of a more complex tissue structure. In addition, this technology could potentially be used to test different biomaterials in conjunction with drug eluting strategy to engineer tissue formation. Further work is needed to scale up this technology to large-scale production of cell toroids suitable for various applications ranging from drug discovery to 3D bio printing.

Materials and Methods

Cell culture. The green fluorescent protein (GFP) expressing immortalized mouse OECs were obtained from Prof Filip Lim, Universidad Autonoma de Madrid, Madrid, Spain. Cells were cultured in DMEM/F12 (Life Technologies) supplemented with 10% FBS (vol/vol), 2 μ M forskolin (Sigma), 20 μ g ml⁻¹ pituitary extract (Gibco), 10 ng ml⁻¹ FGF-2 (PeproTech), 10 ng ml⁻¹ EGF (PeproTech) and 0.5% (vol/vol) gentamicin (Life Technologies). Cells at 75% confluence were harvested from in T25 flasks by washing twice with HBSS (Life Technologies) and detached with TrypLE Express (Life Technologies) for 5 minutes at 37 °C. Subsequently, the enzymatic reaction was stopped using 2 mL 10% FBS media and the solution centrifuged at 1000 rpm for 5 min. The OECs were grown by changing media every 2 days.

Preparation low-melting point hydrogel. In the experiments of this paper, agarose serves as the hydrogel. An amount of 0.01 g low-melting-point agarose (Invitrogen) was placed into a 10-mL falcon tube and diluted into 10 ml HBSS to make a 1% agarose solution by careful heating with microwave oven until boiling, stirred to facilitate complete dissolution. When the temperature decreased to 40 °C, the agarose solution was further diluted in 1:1 ratio with a medium, or medium containing 10 ng/mL epidermal growth factor (EGF), and suspended in the 1.5-mL Eppendorf tube. The Eppendorf tube was heated at 37.5 °C using a hot plate inside a hood. The mixture was heated on a hot plate in the cell culture hood until boiling. Subsequent stirring facilitates the complete dissolution of the agarose. Most experiments in this paper utilized 0.5% agarose.

Preparation of hydrogel sphere. Polytetrafluoroethylene (PTFE) powder with particle sizes of 1 μ m (Sigma-Aldrich, product number 430935) was prepared inside a 6-well plate. A micropipette was then used to dispense 5 μ L of 0.5% agarose on the hydrophobic powder bed. The droplet was gently shaken in a circular motion for 2 minutes to form a hydrogel liquid marble. The hydrogel liquid marble was then kept for 3 minutes to ensure agarose completely solidifies to form the hydrogel sphere.

Preparation of encapsulated hydrogel sphere with cells. A pre-determined number of cells (1000 to 5000 cells/ μ L) in 10 μ L were dispensed vertically on top of a sessile hydrogel liquid marble on a PTFE powder bed. The PTFE particles coated on hydrogel disperse and migrate out to the liquid-air interface, once merging with the second droplet containing cells. Finally, the compound droplet was rolled on the powder bed in a circular motion for two minutes to form the larger liquid marble containing both cells and the hydrogel sphere. Figure 1A shows the bioreactor system with a hydrogel sphere embedded in the liquid marble.

Toroid geometry measurement. We calculated the aspect ratio and the volume using the values of major (R) and minor (r) radii of the toroid. The radii values were determined based on average value obtain from ten measurements from each toroid tissue. The total number of toroids used in each group were n = 5. We used the equation $V = 2\pi^2 Rr^2$ and $A = 4\pi^2 Rr$ for calculating the volume and area, respectively. The aspect ratio is defined as R/r. All measurements were carried out using ImageJ software.

Cell toroid closure assay. For three-dimensional wound closure assays, individual cell toroid was harvested from the liquid marble. Subsequently, a media volume of 50 μ L was dispensed using p1000 pipette tips into each well of a 96-well plate containing broken liquid marble followed by careful suspension and picking the cell toroids. Harvested cell toroids were transferred into a 384-well plate with non-adherence surface. Finally, a media volume of 50 μ L containing 10 ng/mL GDNF or test drugs were dispensed into the well. Bright field and fluorescent images were obtained using a microscope (Olympus IX70) equipped with the Axiocan camera. Fluorescent images were captured at 6-hour intervals for 24 hours. Images were analysed using ImageJ software (NIH, USA).

References

- Vadivelu, R., Kamble, H., Shiddiky, M. & Nguyen, N.-T. Microfluidic technology for the generation of cell spheroids and their applications. *Micromachines* **8**, 94, <https://doi.org/10.3390/mi8040094> (2017).
- Kessel, S. *et al.* High-Throughput 3D Tumor Spheroid Screening Method for Cancer Drug Discovery Using Celigo Image Cytometry. *J Lab Autom*, doi:<https://doi.org/10.1177/2211068216652846> (2016).
- Horvath, P. *et al.* Screening out irrelevant cell-based models of disease. *Nat Rev Drug Discov*, doi:<https://doi.org/10.1038/nrd.2016.175> (2016).
- Nantasanti, S., de Bruin, A., Rothuizen, J., Penning, L. C. & Schotanus, B. A. Concise Review: Organoids Are a Powerful Tool for the Study of Liver Disease and Personalized Treatment Design in Humans and Animals. *Stem Cells Transl Med* **5**, 325–330, <https://doi.org/10.5966/sctm.2015-0152> (2016).
- Knight, E. & Przyborski, S. Advances in 3D cell culture technologies enabling tissue-like structures to be created *in vitro*. *J Anat* **227**, 746–756, <https://doi.org/10.1111/joa.12257> (2015).
- Lee, G. H., Lee, J. S., Wang, X. & Lee, S. H. Bottom-Up Engineering of Well-Defined 3D Microtissues Using Microplatforms and Biomedical Applications. *Adv Healthc Mater* **5**, 56–74, <https://doi.org/10.1002/adhm.201500107> (2016).
- Anastasov, N. *et al.* A 3D-microtissue-based phenotypic screening of radiation resistant tumor cells with synchronized chemotherapeutic treatment. *BMC Cancer* **15**, 466, <https://doi.org/10.1186/s12885-015-1481-9> (2015).

8. Vrij, E. J. *et al.* 3D high throughput screening and profiling of embryoid bodies in thermoformed microwell plates. *Lab Chip* **16**, 734–742, <https://doi.org/10.1039/c5lc01499a> (2016).
9. Vrij, E. *et al.* Directed Assembly and Development of Material-Free Tissues with Complex Architectures. *Adv Mater* **28**, 4032–4039, <https://doi.org/10.1002/adma.201505723> (2016).
10. Masuda, T. *et al.* A microfabricated platform to form three-dimensional toroidal multicellular aggregate. *Biomed Microdevices* **14**, 1085–1093, <https://doi.org/10.1007/s10544-012-9713-0> (2012).
11. Napolitano, A. P., Chai, P., Dean, D. M. & Morgan, J. R. Dynamics of the self-assembly of complex cellular aggregates on micromolded nonadhesive hydrogels. *Tissue Eng* **13**, 2087–2094, <https://doi.org/10.1089/ten.2006.0190> (2007).
12. Youssef, J., Nurse, A. K., Freund, L. B. & Morgan, J. R. Quantification of the forces driving self-assembly of three-dimensional microtissues. *Proc Natl Acad Sci USA* **108**, 6993–6998, <https://doi.org/10.1073/pnas.1102559108> (2011).
13. Sandu, I. & Fleaca, C. T. The influence of gravity on the distribution of the deposit formed onto a substrate by sessile, hanging, and sandwiched hanging drop evaporation. *J Colloid Interface Sci* **358**, 621–625, <https://doi.org/10.1016/j.jcis.2011.03.052> (2011).
14. Ooi, C. H. *et al.* Evaporation of Ethanol-Water Binary Mixture Sessile Liquid Marbles. *Langmuir* **32**, 6097–6104, <https://doi.org/10.1021/acs.langmuir.6b01272> (2016).
15. Sarvi, F. *et al.* Cardiogenesis of embryonic stem cells with liquid marble micro-bioreactor. *Adv Healthc Mater* **4**, 77–86, <https://doi.org/10.1002/adhm.201400138> (2015).
16. Khaw, M. K. *et al.* Digital microfluidics with a magnetically actuated floating liquid marble. *Lab Chip* **16**, 2211–2218, <https://doi.org/10.1039/c6lc00378h> (2016).
17. Ooi, C. H. *et al.* Floating mechanism of a small liquid marble. *Sci Rep* **6**, 21777, <https://doi.org/10.1038/srep21777> (2016).
18. Ooi, C. H., Vadivelu, R. K., St. John, J., Dao, D. V. & Nguyen, N. T. Deformation of a floating liquid marble. *Soft Matter* **11**, 4576–4583, <https://doi.org/10.1039/c4sm02882a> (2015).
19. Vadivelu, R. K. *et al.* Generation of three-dimensional multiple spheroid model of olfactory ensheathing cells using floating liquid marbles. *Sci Rep* **5**, 15083, <https://doi.org/10.1038/srep15083> (2015).
20. Paul, C. D., Hung, W. C., Wirtz, D. & Konstantopoulos, K. Engineered Models of Confined Cell Migration. *Annu Rev Biomed Eng* **18**, 159–180, <https://doi.org/10.1146/annurev-bioeng-071114-040654> (2016).
21. Driscoll, M. K. & Danuser, G. Quantifying Modes of 3D Cell Migration. *Trends Cell Biol* **25**, 749–759, <https://doi.org/10.1016/j.tcb.2015.09.010> (2015).
22. Keely, P. & Nain, A. Capturing relevant extracellular matrices for investigating cell migration. *F1000Res* **4**, doi:<https://doi.org/10.12688/f1000research.6623.1> (2015).
23. Jakab, K., Neagu, A., Mironov, V., Markwald, R. R. & Forgacs, G. Engineering biological structures of prescribed shape using self-assembling multicellular systems. *Proc Natl Acad Sci USA* **101**, 2864–2869, <https://doi.org/10.1073/pnas.0400164101> (2004).
24. Thomas, D. *et al.* Scaffold and scaffold-free self-assembled systems in regenerative medicine. *Biotechnol Bioeng* **113**, 1155–1163, <https://doi.org/10.1002/bit.25869> (2016).
25. Yang, Z. H. *et al.* A novel possible strategy based on self-assembly approach to achieve complete periodontal regeneration. *Artif Organs* **34**, 603–609, <https://doi.org/10.1111/j.1525-1594.2009.00991.x> (2010).
26. Hsu, S. H. & Hsieh, P. S. Self-assembled adult adipose-derived stem cell spheroids combined with biomaterials promote wound healing in a rat skin repair model. *Wound Repair Regen* **23**, 57–64, <https://doi.org/10.1111/wrr.12239> (2015).
27. Friedl, P. & Brocker, E. B. The biology of cell locomotion within three-dimensional extracellular matrix. *Cell Mol Life Sci* **57**, 41–64, <https://doi.org/10.1007/s000180050498> (2000).
28. Liu, L., Luo, Q., Sun, J. & Song, G. Nucleus and nucleus-cytoskeleton connections in 3D cell migration. *Exp Cell Res*, doi:<https://doi.org/10.1016/j.yexcr.2016.09.001> (2016).
29. DuRaine, G. D., Brown, W. E., Hu, J. C. & Athanasiou, K. A. Emergence of scaffold-free approaches for tissue engineering musculoskeletal cartilages. *Ann Biomed Eng* **43**, 543–554, <https://doi.org/10.1007/s10439-014-1161-y> (2015).
30. Evensen, N. A. *et al.* Development of a high-throughput three-dimensional invasion assay for anti-cancer drug discovery. *PLoS One* **8**, e82811, <https://doi.org/10.1371/journal.pone.0082811> (2013).
31. Jiang, L. Y., Lv, B. & Luo, Y. The effects of an RGD-PAMAM dendrimer conjugate in 3D spheroid culture on cell proliferation, expression and aggregation. *Biomaterials* **34**, 2665–2673, <https://doi.org/10.1016/j.biomaterials.2013.01.003> (2013).
32. Wan, A. C. Recapitulating Cell-Cell Interactions for Organoid Construction - Are Biomaterials Dispensable? *Trends Biotechnol* **34**, 711–721, <https://doi.org/10.1016/j.tibtech.2016.02.015> (2016).
33. Rommerswinkel, N., Niggemann, B., Keil, S., Zanker, K. S. & Dittmar, T. Analysis of cell migration within a three-dimensional collagen matrix. *J Vis Exp*, e51963, doi:<https://doi.org/10.3791/51963> (2014).
34. Whitehead, B. C., Bezuidenhout, D., Chokoza, C., Davies, N. H. & Goetsch, K. P. Cast Tube Assay: A 3-D *in vitro* assay for visualization and quantification of horizontal chemotaxis and cellular invasion. *Biotechniques* **61**, 66–72, <https://doi.org/10.2144/000114442> (2016).
35. Sakar, M. S. *et al.* Cellular forces and matrix assembly coordinate fibrous tissue repair. *Nat Commun* **7**, 11036, <https://doi.org/10.1038/ncomms11036> (2016).
36. Gosiewska, A. *et al.* Development of a three-dimensional transmigration assay for testing cell-polymer interactions for tissue engineering applications. *Tissue Eng* **7**, 267–277, <https://doi.org/10.1089/10763270152044134> (2001).
37. Chung, S. *et al.* Cell migration into scaffolds under co-culture conditions in a microfluidic platform. *Lab on a Chip* **9**, 269–275 (2009).
38. Jiang, Z. *et al.* Enhanced Migration of Neural Stem Cells by Microglia Grown on a Three-Dimensional Graphene Scaffold. *ACS Appl Mater Interfaces* **8**, 25069–25077, <https://doi.org/10.1021/acsami.6b06780> (2016).
39. Timm, D. M. *et al.* A high-throughput three-dimensional cell migration assay for toxicity screening with mobile device-based macroscopic image analysis. *Sci Rep* **3**, 3000, <https://doi.org/10.1038/srep03000> (2013).
40. Li, L. *et al.* Effects of transplantation of olfactory ensheathing cells in chronic spinal cord injury: a systematic review and meta-analysis. *Eur Spine J* **24**, 919–930, <https://doi.org/10.1007/s00586-014-3416-6> (2015).
41. Tabakow, P. *et al.* Functional regeneration of supraspinal connections in a patient with transected spinal cord following transplantation of bulbar olfactory ensheathing cells with peripheral nerve bridging. *Cell Transplant* **23**, 1631–1655, <https://doi.org/10.3727/096368914X685131> (2014).
42. Delaviz, H. *et al.* Transplantation of olfactory mucosa improve functional recovery and axonal regeneration following sciatic nerve repair in rats. *Iran Biomed J* **12**, 197–202 (2008).
43. Woodhall, E., West, A. K. & Chuah, M. I. Cultured olfactory ensheathing cells express nerve growth factor, brain-derived neurotrophic factor, glia cell line-derived neurotrophic factor and their receptors. *Brain Res Mol Brain Res* **88**, 203–213 (2001).
44. Cao, L. *et al.* Glial cell line-derived neurotrophic factor promotes olfactory ensheathing cells migration. *Glia* **54**, 536–544, <https://doi.org/10.1002/glia.20403> (2006).
45. Wang, Y. *et al.* Brain-derived Neurotrophic Factor Promotes the Migration of Olfactory Ensheathing Cells Through TRPC Channels. *Glia* **64**, 2154–2165, <https://doi.org/10.1002/glia.23049> (2016).
46. Bormashenko, E. Liquid Marbles, Elastic Nonstick Droplets: From Minireactors to Self-Propulsion. *Langmuir* **33**, 663–669, <https://doi.org/10.1021/acs.langmuir.6b03231> (2017).
47. Li, X. *et al.* EGF and curcumin co-encapsulated nanoparticle/hydrogel system as potent skin regeneration agent. *Int J Nanomedicine* **11**, 3993–4009, <https://doi.org/10.2147/IJN.S104350> (2016).

48. Dogan, A. K., Gumusderelioglu, M. & Aksoz, E. Controlled release of EGF and bFGF from dextran hydrogels *in vitro* and *in vivo*. *J Biomed Mater Res B Appl Biomater* **74**, 504–510, <https://doi.org/10.1002/jbm.b.30231> (2005).
49. Lao, G. *et al.* Controlled release of epidermal growth factor from hydrogels accelerates wound healing in diabetic rats. *J Am Podiatr Med Assoc* **102**, 89–98 (2012).
50. Crank, J. *The mathematics of diffusion*. 2d edn, (Clarendon Press, 1975).
51. Roam, J. L., Nguyen, P. K. & Elbert, D. L. Controlled release and gradient formation of human glial-cell derived neurotrophic factor from heparinated poly(ethylene glycol) microsphere-based scaffolds. *Biomaterials* **35**, 6473–6481, <https://doi.org/10.1016/j.biomaterials.2014.04.027> (2014).
52. Latifi-Pupovci, H. *et al.* *In vitro* migration and proliferation (“wound healing”) potential of mesenchymal stromal cells generated from human CD271(+) bone marrow mononuclear cells. *J Transl Med* **13**, 315, <https://doi.org/10.1186/s12967-015-0676-9> (2015).
53. Pellitteri, R. *et al.* Viability of olfactory ensheathing cells after hypoxia and serum deprivation: Implication for therapeutic transplantation. *J Neurosci Res* **92**, 1757–1766, <https://doi.org/10.1002/jnr.23442> (2014).
54. Heo, Y. S. *et al.* Characterization and resolution of evaporation-mediated osmolality shifts that constrain microfluidic cell culture in poly (dimethylsiloxane) devices. *Analytical chemistry* **79**, 1126–1134 (2007).
55. Choudhary, M., Shalaby, A. & Al-Omran, A. Water holding capacity and evaporation of calcareous soils as affected by four synthetic polymers. *Communications in Soil Science & Plant Analysis* **26**, 2205–2215 (1995).
56. Hoare, T. R. & Kohane, D. S. Hydrogels in drug delivery: progress and challenges. *Polymer* **49**, 1993–2007 (2008).
57. He, C., Kim, S. W. & Lee, D. S. *In situ* gelling stimuli-sensitive block copolymer hydrogels for drug delivery. *Journal of controlled release* **127**, 189–207 (2008).
58. Haessler, U., Kalinin, Y., Swartz, M. A. & Wu, M. An agarose-based microfluidic platform with a gradient buffer for 3D chemotaxis studies. *Biomedical microdevices* **11**, 827–835 (2009).
59. Abhyankar, V. V. *et al.* A platform for assessing chemotactic migration within a spatiotemporally defined 3D microenvironment. *Lab on a Chip* **8**, 1507–1515 (2008).
60. Youssef, J., Nurse, A. K., Freund, L. & Morgan, J. R. Quantification of the forces driving self-assembly of three-dimensional microtissues. *Proceedings of the National Academy of Sciences* **108**, 6993–6998 (2011).

Acknowledgements

We acknowledge the funding support of the Australian Research Council for the discovery grant DP170100277.

Author Contributions

R.K.V. and N.T.N. designed the experiments and wrote the paper. R.K.V. carried out the cell culture experiments. H.K. developed the numerical model and carried out the simulation for the distribution of the growth factor. R.K.V. and A.M. evaluated the data from the recorded images. All authors have contributed, seen and approved the manuscript.

Additional Information

Competing Interests: The authors declare that they have no competing interests.

Publisher's note: Springer Nature remains neutral with regard to jurisdictional claims in published maps and institutional affiliations.



Open Access This article is licensed under a Creative Commons Attribution 4.0 International License, which permits use, sharing, adaptation, distribution and reproduction in any medium or format, as long as you give appropriate credit to the original author(s) and the source, provide a link to the Creative Commons license, and indicate if changes were made. The images or other third party material in this article are included in the article's Creative Commons license, unless indicated otherwise in a credit line to the material. If material is not included in the article's Creative Commons license and your intended use is not permitted by statutory regulation or exceeds the permitted use, you will need to obtain permission directly from the copyright holder. To view a copy of this license, visit <http://creativecommons.org/licenses/by/4.0/>.

© The Author(s) 2017